Biomechanical Strain Exacerbates Inflammation on a Progeria-on-a-Chip Model

João Ribas, Yu Shrike Zhang, Patrícia R. Pitrez, Jeroen Leijten, Mario Miscuglio, Jeroen Rouwkema, Mehmet Remzi Dokmeci, Xavier Nissan, Lino Ferreira, and Ali Khademhosseini**

Organ-on-a-chip platforms seek to recapitulate the complex microenvironment of human organs using miniaturized microfluidic devices. Besides modeling healthy organs, these devices have been used to model diseases, yielding new insights into pathophysiology. Hutchinson-Gilford progeria syndrome (HGPS) is a premature aging disease showing accelerated vascular aging, leading to the death of patients due to cardiovascular diseases. HGPS targets primarily vascular cells, which reside in mechanically active tissues. Here, a progeria-on-a-chip model is developed and the effects of biomechanical strain are examined in the context of vascular aging and disease. Physiological strain induces a contractile phenotype in primary smooth muscle cells (SMCs), while a pathological strain induces a hypertensive phenotype similar to that of angiotensin II treatment. Interestingly, SMCs derived from human induced pluripotent stem cells of HGPS donors (HGPS iPS-SMCs), but not from healthy donors, show an exacerbated inflammatory response to strain. In particular, increased levels of inflammation markers as well as DNA damage are observed. Pharmacological intervention reverses the strain-induced damage by shifting gene expression profile away from inflammation. The progeria-on-a-chip is a relevant platform to study biomechanics in vascular biology, particularly in the setting of vascular disease and aging, while simultaneously facilitating the discovery of new drugs and/or therapeutic targets.

J. Ribas, Dr. Y. S. Zhang, Dr. J. Leijten, M. Miscuglio, Dr. M. R. Dokmeci, Prof. A. Khademhosseini
Biomaterials Innovation Research Center
Division of Engineering in Medicine
Department of Medicine
Brigham and Women's Hospital
Harvard Medical School
Cambridge, MA 02139, USA
E-mail: alik@bwh.harvard.edu

J. Ribas, Dr. Y. S. Zhang, Dr. J. Leijten, M. Miscuglio, Dr. M. R. Dokmeci, Prof. A. Khademhosseini
Harvard-MIT Division of Health Sciences and Technology
Massachusetts Institute of Technology
Cambridge, MA 02139, USA

J. Ribas
Doctoral Program in Experimental Biology and Biomedicine
Center for Neuroscience and Cell Biology
Institute for Interdisciplinary Research
University of Coimbra
3030-789 Coimbra, Portugal

Dr. P. R. Pitrez, Prof. L. Ferreira
CNC-Centre for Neuroscience and Cell Biology
University of Coimbra
3030-789 Coimbra, Portugal
E-mail: lino@biocant.pt

Dr. P. R. Pitrez, Prof. L. Ferreira
Institute for Interdisciplinary Research
University of Coimbra
3030-789 Coimbra, Portugal

Dr. J. Leijten
Department of Developmental BioEngineering
MIRA Institute for Biomedical Technology
and Technical Medicine
University of Twente
7500 AE Enschede, The Netherlands

Dr. J. Rouwkema
Department of Biomechanical Engineering
MIRA Institute for Biomedical Technology and Technical Medicine
University of Twente
7500 AE Enschede, The Netherlands

Dr. X. Nissan
CECS, INSERM U861
I-STEM
AFM
Institute for Stem Cell Therapy and Exploration of Monogenic Diseases
28 Rue Henri Desbrueres, 91100 Corbeil-Essones, France

Prof. A. Khademhosseini
Department of Physics
King Abdulaziz University
Jeddah 21569, Saudi Arabia

Prof. A. Khademhosseini
Department of Bioindustrial Technologies
College of Animal Bioscience and Technology
Konkuk University
Hwayang-dong, Gwangjin-gu, Seoul 143-701, Republic of Korea

DOI: 10.1002/smll.201603737

1. Introduction

The naturally occurring biomechanical strains in blood vessels translate via mechanotransduction into behavioral changes of vascular smooth muscle cells (SMCs) and endothelial cells (ECs). Whereas ECs are primarily exposed to fluid shear stress, SMCs are mainly exposed to cyclic biomechanical strain, which plays a key role in controlling the tone of the vessel and concomitant blood pressure.[1] In a healthy arterial wall, SMCs experience cyclic biomechanical strain of 9%,[2] while SMCs under pathological conditions experience strains of up to ≈15%.[3] In vitro, several studies conducted have utilized uniaxial strain values in the order of 5%–25%.[4] These studies revealed that cyclical biomechanical strain in SMCs is transduced by integrins[5] and results in the acquisition of a contractile phenotype reminiscent of the in vivo phenotype.[4,6,7] Pathologic levels of biomechanical strain can increase reactive oxygen species (ROS) levels as well as induce expression of vascular injury and inflammation markers.[4,8] Accumulated levels of such markers are hallmarks of vascular disease and progressively increase during aging,[9,10] leading to further worsening of pathology.

Currently there is no dedicated in vitro microfluidic system with SMCs to study the impact of biomechanics on aging and vascular diseases such as hypertension. In the past few years, the lack of appropriate in vitro models has motivated the need for the development of microfluidic organ-on-a-chip models[11–13] that are able to recapitulate the complex in vivo biological parameters. Integration with microfluidic devices makes these platforms uniquely suited to apply physiologically relevant biomechanical strain, shear stress, and transmural pressure, and/or provide 3D environments. To date, some microfluidic models have been developed to apply biomechanical strain mimicking the lung,[14–16] gut,[17–19] and blood vessels,[20–24] but have not been applied in the context of human vascular aging.

Recently, stem cell technologies have facilitated the generation of aged cells.[25] Hutchinson-Gilford progeria syndrome (HGPS) is a rare genetic disorder caused by a mutant form of the nuclear protein lamin A—progerin.[26,27] HGPS patients suffer from premature and accelerated aging,[25,28–31] while accumulation of progerin also occurs during physiological aging. Notably, HGPS targets primarily vascular cells,[32] which are mechanically active. Induced pluripotent stem cells (iPSCs) generated from HGPS fibroblasts have been used to recapitulate normal aging in an accelerated fashion,[29,30,33–35] proving to be a valuable tool to study vascular aging and thus facilitate the discovery of novel treatments.[36,37] However, accurate in vitro models must take into account the interplay between biomechanical strain and the behavior of aged cells.

Here, we set out to develop a novel progeria-on-a-chip model that would capture blood vessel biomechanical dynamics on chip. Within this device, we exposed healthy iPS-SMCs and HGPS iPS-SMCs to normal and pathological strains to study the interplay between biomechanical strain and vascular aging. Models that combine biomechanics and vascular aging are crucial tools toward understanding vascular disease/aging and developing new therapies.

2. Results

2.1. Recapitulating Blood Vessel Dynamics on Chip

Blood vessels are constantly exposed to cyclic mechanical stretch (**Figure 1**A) varying from the normal 9% relative strain in healthy individuals[2] to the pathological 15% relative strain.[3] Studies conducted in vitro used values in the order of 5%–25%,[4] with the range of 5%–10% being considered physiological and >15% pathological strain. To recapitulate the cyclic mechanical deformation experienced by SMCs in the arterial wall of blood vessels we have developed a novel microfluidic polydimethylsiloxane (PDMS) device (Figure 1B–E). The device consists of a top fluidic channel with an underlying vacuum channel that is separated by a 123.5 ± 3.0 μm PDMS membrane (Figure 1B and Figure S1, Supporting Information). The fabrication process is simple (Figure 1C–D) and relies on the creation of a three-layer device, the top fluidic channel, a middle thin PDMS membrane, and a bottom vacuum channel. Cells are cultured on top of the membrane (Figure 1F), which is deformed by applying different pressure drops on the bottom channel (Movie S1, Supporting Information). Previous approaches used pressure drops on side channels to stretch a membrane over a central post,[22,38,39] or positive pressure to bulge a membrane.[40,41] The device measures 40 mm × 18 mm (Figure 1E), is optically transparent, and fits a standard glass slide for easy microscopic visualization. The fluidic channel has a straight region measuring 25 mm × 1 mm. To facilitate channel alignment during assembly of the PDMS layers, the bottom layer was 0.2 mm wider. The device was designed to be usable in any laboratory setting: pressure drops used are obtained from a laboratory vacuum line, and cell seeding onto the device can be achieved by manually pipetting a cell suspension inside the fluidic channel. We have used this novel device to characterize the vascular response of healthy and HGPS iPS-SMCs to different levels of biomechanical strain (Figure 1G).

To characterize the device, we determined the membrane deformation in situ and in silico. Cross-sectional views of the microfluidic device under different amounts of vacuum pressure ranging from 0 to 50 kPa demonstrated a pressure-dependent increase in membrane deformation (**Figure 2**A). The approach used to show in situ membrane deformation has not been demonstrated before and allows immediate and direct visualization of membrane deformation. The thickness and mechanical properties of the membrane were tailored to function under low pressures while achieving the required strains. A pressure drop of 10 kPa was found to average to 9% ± 2% strain, 20 kPa to 16% ± 1%, and 30 kPa to 24% ± 2% (Figure 2B). In silico modeling of the membrane deformation demonstrated similar results in the range of 0–30 kPa (Figure S2, Supporting Information). Indeed, a strong correlation was found between cross-sectional measurements and simulation data (Figure 2B; Pearson's correlation of $r = 0.9825$). Moreover, we mapped the variability in mechanical strain by characterizing the surface strain (Figure S2, Supporting Information). Additionally, we have simulated the effect

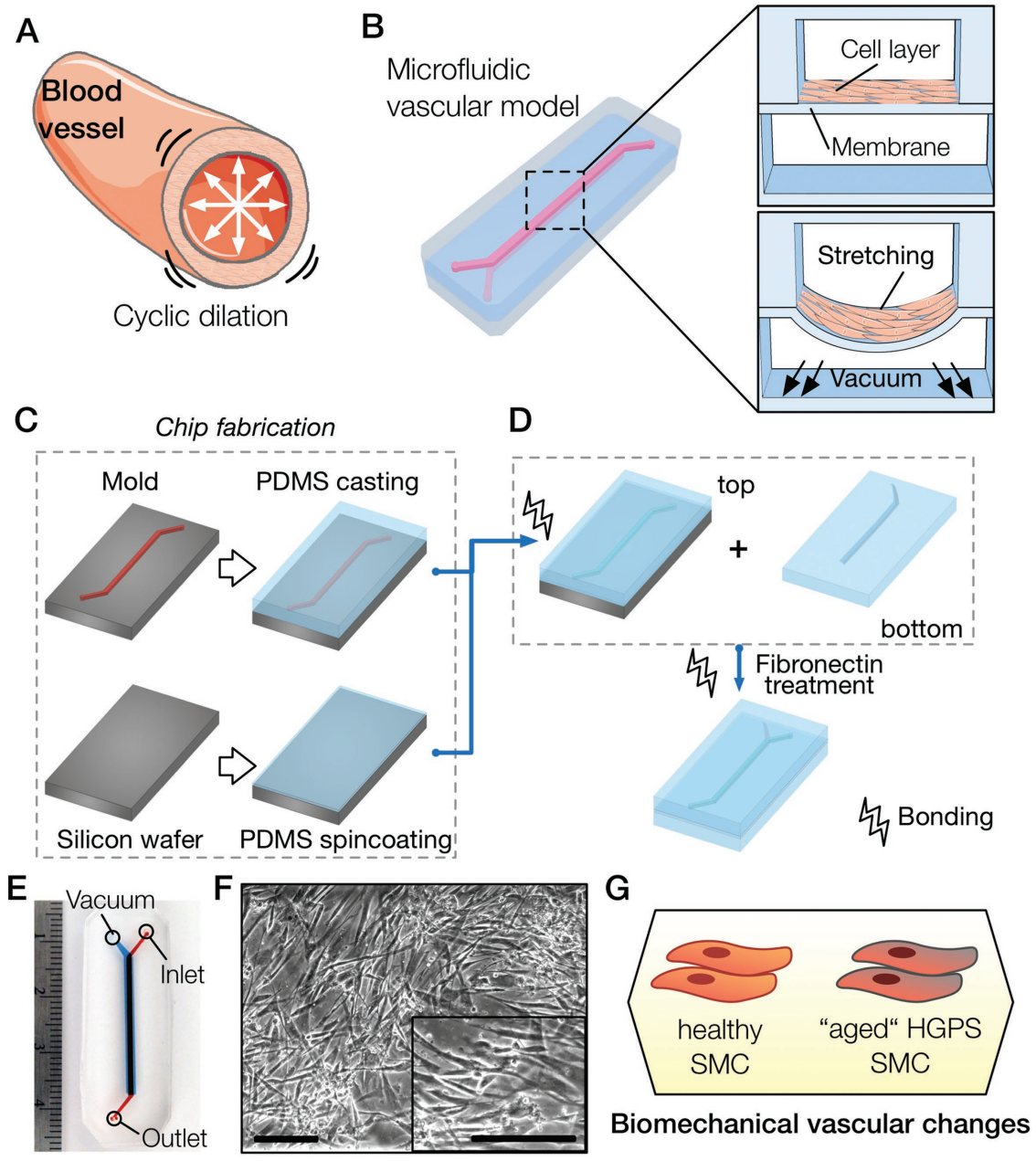

Figure 1. Recapitulation of blood vessel dynamics on chip. A) Blood vessels experience cyclic strain due to the pulsatile nature of blood flow. B) Biomimetic microfluidic vascular model containing two overlapping channels. A cross-sectional view of the microfluidic device shows the cell layer cultured on top of the PDMS membrane and a view during vacuum stimulation shows the downward membrane deformation. C) The first step of the chip fabrication containing the casting of PDMS (10:1 ratio) on an acetal resin mold and the spin-coating of PDMS (20:1 ratio) to generate a thin membrane on top of a silicon wafer. D) The top slab and membrane portions of the PDMS device are bonded using oxygen plasma and then peeled off the silicon wafer. The top part is then bonded to the bottom PDMS slab molded previously, and treated with fibronectin solution to allow cell culture. E) Photograph of the microfluidic channel showing the media inlet, outlet, and the vacuum port. F) Micrographs of SMCs cultured in the microfluidic chip (scale bar represents 250 μm). G) Proposed methodology to unveil strain-related vascular changes in iPS-derived SMCs from healthy and HGPS donors.

of this spatial strain distribution on cells attached to the membrane using micrographs of nuclei within our devices (Figure 2C). In line with our modeling, we observed a gradient strain similar to other reports for microfluidic strain devices.[14] Importantly, we have also verified that the strain applied was mostly uniaxial (Figure 2D). We used the average strain values and analyzed the entire cell population inside the microfluidic device.

2.2. Biomechanical Strain Induced Cell Reorientation and a Contractile Phenotype in SMCs

Mechanical stimulation regulates morphology and function of SMCs.[3] The lack of mechanical strain in static cultures induces SMCs to shift toward a dedifferentiated phenotype, which is characterized by a higher proliferative state, higher protein synthesis, and relatively circular cell shape.[3,4,42]

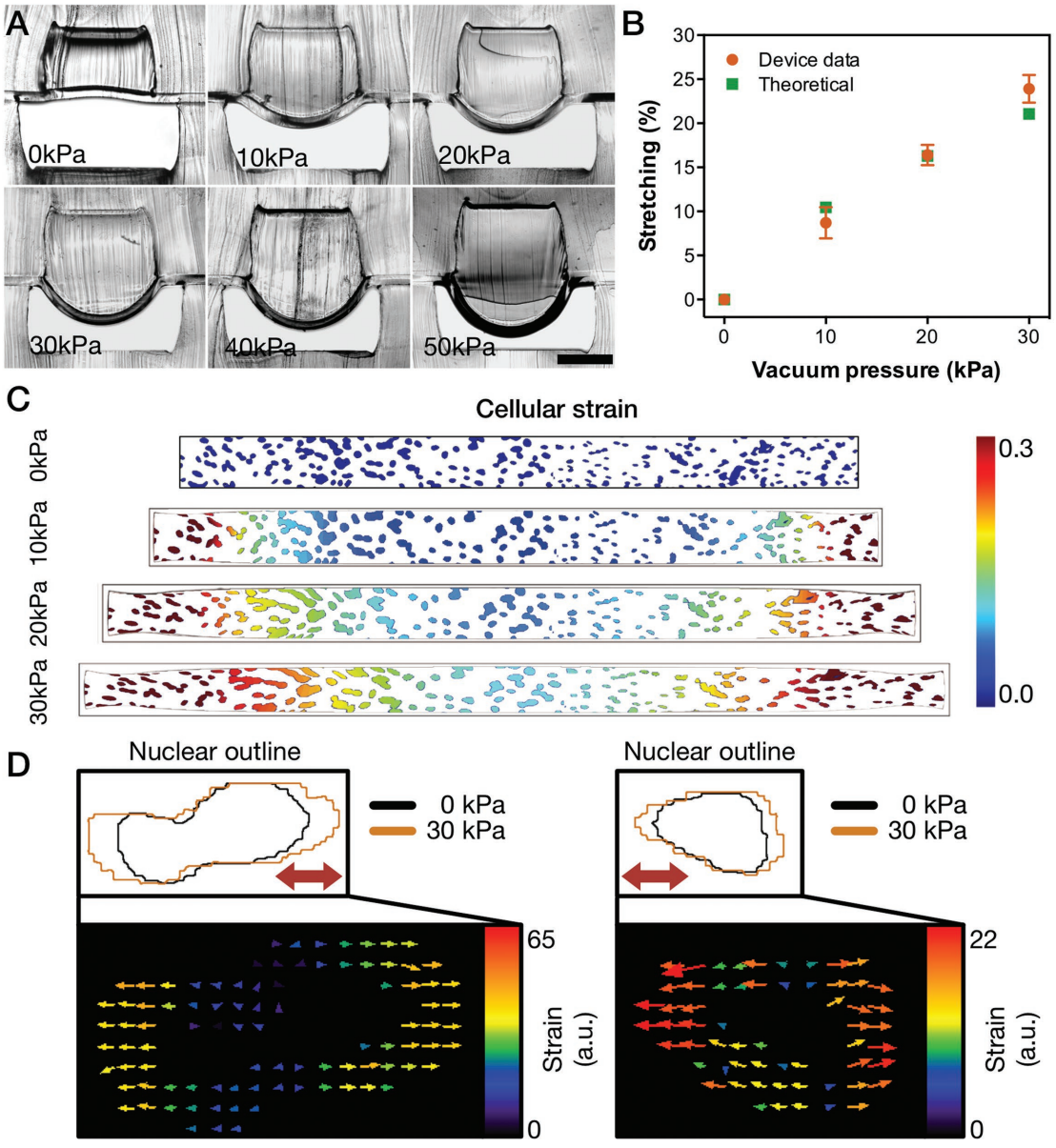

Figure 2. Characterization of stretch capabilities of microfluidic device. A) Cross-sectional view of microfluidic device and membrane deformation under different amounts of pressure drop (scale bar represents 500 µm). B) Comparison of the overall strain on the *y*-axis between cross-sectional measurements and theoretical computational simulation (results represent mean ± SD of $n = 5$). C) Computational simulation of the strain on a 1 mm × 0.1 mm membrane section overlaid with a representative nuclei image under different levels of pressure drop. D) Two representative nuclear outlines of cells under 0 and 30 kPa and respective vector displacement maps (thick red arrows in the top panels indicate strain direction).

Upon mechanical stimulation, cells acquire a contractile phenotype that is reminiscent of the in vivo state. SMCs under cyclic mechanical strain reorient perpendicular to the strain direction.[43,44] We examined the morphology, orientation, and expression of contractile markers by SMCs under normal and hypertensive mechanical strains. Cells were cultured for 24 h under cyclic mechanical strain in a microfluidic channel coated with fibronectin. This coating was chosen because SMCs are more responsive to the cyclic strain on fibronectin-coated substrates rather than other extra cellular matrix (ECM) proteins.[42] We cultured cells for 24 h to observe early effects of strain, whereas other studies cultured cells for 48 or 72 h.[42,45] SMCs under no mechanical strain exhibited a random angle orientation distribution (**Figure 3**A). Strained cells reoriented perpendicular to the direction of strain and increased their aspect ratio (Figure 3B,C), with a magnitude-dependent effect. Indeed, the angle orientation distribution of SMCs became narrower and closer to 0° as the stretch was increased from 9% to 16% strain (Figure 3D–F). Cell shape analysis revealed a decrease in cell width (Figure 3G and Figure S3, Supporting Information), while no change was observed in cell length (Figure S3, Supporting Information), resulting in an overall increase in the aspect ratio of the cells (Figure 3H). SM22α and β1-integrin are enriched in contractile SMCs.[6] Besides, β1 and α5-integrins mediate intracellular signal mechanotransduction via adhesion to fibronectin.[3–5,42]

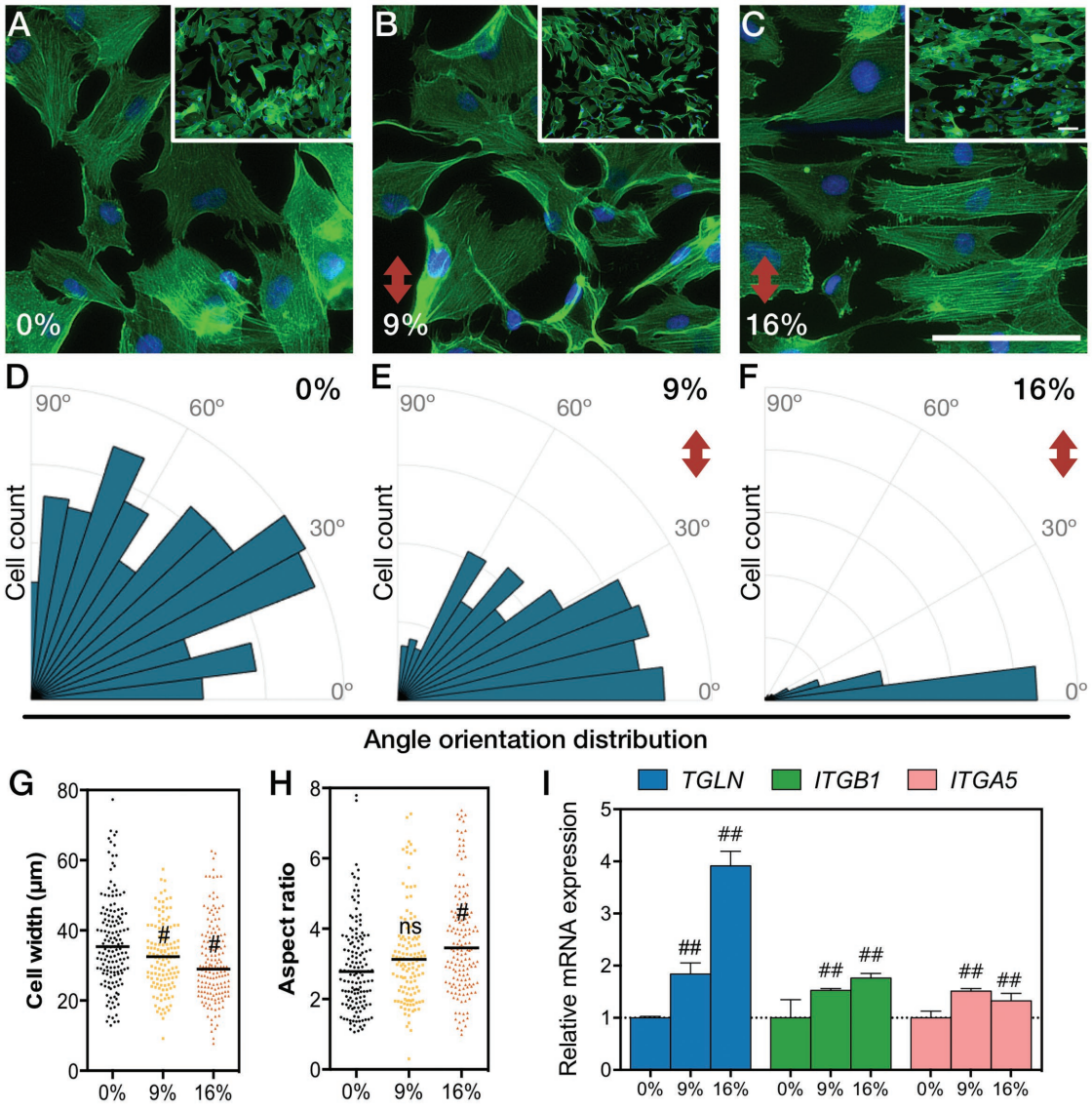

Figure 3. Strain induces cytoskeletal reorientation and contractile phenotype markers on chip. A–C) Micrographs of F-actin stained cells under different amounts of strain for 24 h. Cells exposed to different amounts of strain were quantified on D–F) angle orientation distribution, G) cell width, and H) aspect ratio (#: $P < 0.01$; ns: not significant; scale bars represent 100 μm and the red arrow indicates direction of strain). Relative mRNA expression levels of *TAGLN* (SM22α gene), *ITGB1* (β1-integrin gene), and *ITGA5* (α5-integrin gene) I) (bars represent mean ± SD of $n = 5$; ##, $P < 0.01$).

Therefore, to evaluate the impact of cyclic stretching in the phenotype of SMCs and their mechanotransduction responsiveness, we measured the expression levels of *TAGLN* (encoding SM22α), *ITGB1* (encoding β1-integrin), and *ITGA5* (encoding α5-integrin) gene transcripts by real-time quantitative polymerase chain reaction (qRT-PCR). We found *TAGLN*, *ITGB1*, and *ITGA5* mRNA upregulated under 9% and 16% strain (Figure 3I). Overall, we confirmed that using our on-chip system SMCs responded to mechanical strain by acquiring a more differentiated contractile phenotype.

2.3. Hypertensive Strain Recapitulates Angiotensin II Induced Phenotype

To evaluate whether a threshold pathological strain induced vascular damage, we analyzed gene expression in cells cultured under strain as compared to static conditions treated with angiotensin II. The renin–angiotensin–aldosterone system is implicated in the development of hypertension and regulates blood pressure in vivo by controlling the vascular tone of SMCs.[46] In this context, angiotensin II has been demonstrated to generate a hypertensive phenotype in SMCs.[46] Caveolin-1 (CAV1), a component of caveolae, is an important mediator of signal transduction[47] and plays a role in mechanotransduction in endothelial cells.[48] Microarray profiles of vascular tissues have identified CAV1 as a potential target marker of hypertension, showing overexpression in both spontaneous and adrenocorticotropic hormone-induced hypertensive rats.[49] Similarly, increased expression of CAV1 and caveolae has been reported in human pulmonary artery hypertension.[50,51] Interleukin-6 (IL-6) is a major proinflammatory cytokine that has been associated with essential

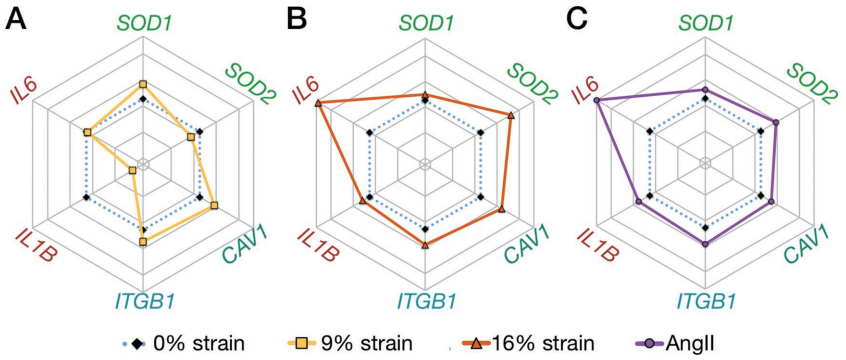

Figure 4. Strain-dependent activation of SMCs recapitulates angiotensin II vascular gene fingerprint. Rose plots of the mRNA expression profiles of SMCs treated for 24 h under A) physiological strain (9%), B) pathological strain (16%), or C) 100×10^{-9} M of angiotensin II [AngII] (mean values of $n = 5$ for 9% and 16% strain, mean values of $n = 3$ for AngII treatment; see Figures S4 and S5 of the Supporting Information for the bar plots and statistical significance).

hypertension,[52] which is overexpressed in human serum of pulmonary hypertension patients[53] and induces hypertension in mice.[54]

Our results showed that culturing SMCs under 9% strain led to minor changes of mRNA expression levels (**Figure 4**A and Figure S4, Supporting Information), with an increase in the cytosolic superoxide dismutase (*SOD1*) and decrease in mitochondrial one (*SOD2*). Importantly, ROS has been implicated in vascular diseases, and angiotensin II is known to increase mitochondrial ROS.[55–58] Both pathological strain (Figure 4B) and 100×10^{-9} M of angiotensin II treatment (Figure 4C and Figure S5, Supporting Information) showed a marked increase in mitochondrial *SOD2*, with a smaller increase in *SOD1*. Interestingly, this observation suggested that under physiological strain ROS was primarily produced in the cytosol. Using the NADPH oxidase inhibitor VAS2870 (20×10^{-6} M)[59] we showed downregulation of the nicotinamide adenine dinucleotide phosphate (NADPH) oxidase subunit *p22phox* and restoration *SOD1* levels, while no change was observed for *SOD2* (Figure S6, Supporting Information).

Our results further showed that CAV1 was upregulated in a strain magnitude-dependent way (Figure S4C, Supporting Information), and a similar increase was shown with angiotensin II treatment (Figure 4C and Figure S5C, Supporting Information). Moreover, we showed increase in ITGB1 with strain and angiotensin II (Figure 4) similar to previously reported results.[60] The proinflammatory markers *IL6* and *IL1B* were significantly increased with hypertensive strain (Figure 4B) and angiotensin II (Figure 4C), but not with physiological strain. Such difference suggested the existence of a strain-dependent threshold that gates the biomechanically induced upregulation of IL-6 expression in SMCs.

Overall, SMCs under pathological strain conditions exhibited a gene expression pattern similar to angiotensin II treatment, with similar responses of ROS, inflammation, and vascular injury genes, although strain alone may not fully recapitulate the effects of angiotensin II. Further studies are required to understand the regulatory pathways of strain and angiotensin II in SMCs, both alone and in combination.

2.4. Healthy and HGPS iPS-SMCs Undergo Cytoskeletal Remodeling upon Biomechanical Strain

Vascular diseases and aging are intimately linked[61] yet rarely studied in an integrated approach. Due to the relation between vascular disease and aging, we examined the influence of biomechanics in an iPS-derived progeria-on-a-chip model. Stem cell-based models represent ideal candidates to study human diseases due to the practical capability of large scale expansion and differentiation.[62] HGPS patients exhibit premature aging, with increased arterial stiffening, expression of proinflammatory markers, risk of atherosclerosis, calcification, and changes in systolic and pulse pressure.[36] HGPS and other accelerated aging syndromes have been established as aging models that recapitulate several aspects of cellular aging.[29,34,36,63] In HGPS, both progerin and lamin A accumulate in the nucleus.[36] We generated SMCs through differentiation[64] of iPS cells derived from HGPS donors (and healthy controls),[35] and evaluated the interplay between biomechanical strain and aging (**Figure 5**A).[36] The generation of iPS cells from HGPS fibroblasts was previously shown to be similar to healthy fibroblast.[35] Importantly, we have characterized the differentiated SMCs derived from HGPS iPS cells, and showed that iPS-SMCs from HGPS donors express significantly higher levels of progerin mRNA (Figure 5B). Considering the focus of the current work, the complete dataset on the characterization of HGPS iPS-SMCs has not been included here and will be reported in another publication in detail. Concordant with the alignment results from SMCs (Figure 3), iPS-derived SMCs from healthy and HGPS donors showed cytoskeletal reorientation upon mechanical stimulation, while nonstimulated cells showed a random distribution (Figure 5C–F).

The accumulation of nuclear lamins and progerin occurs naturally during aging, leading to stiffer and less compliant nuclei.[29,65,66] Besides promoting nuclear architecture changes,[67] this accumulation can further result in alterations in transcription, changes in chromatin structure, and epigenetic changes.[65] However, the mechanism and effects of biomechanical strain in a context of lamin/progerin accumulation are still poorly understood. Using the same approach as Cao et al.,[68] we distinctly evaluated the mRNA levels of *LMNA* and progerin with specific primers by qRT-PCR (Figure S7, Supporting Information). Interestingly, in HGPS iPS-SMCs, physiological strain slightly increased level of progerin while pathological strain decreased progerin and increased *LMNA*. Healthy iPS-SMCs showed an opposite trend with reduced levels of *LMNA* with physiological or pathological strain. We then used an antibody recognizing both lamin A/C and progerin (epitope corresponding to

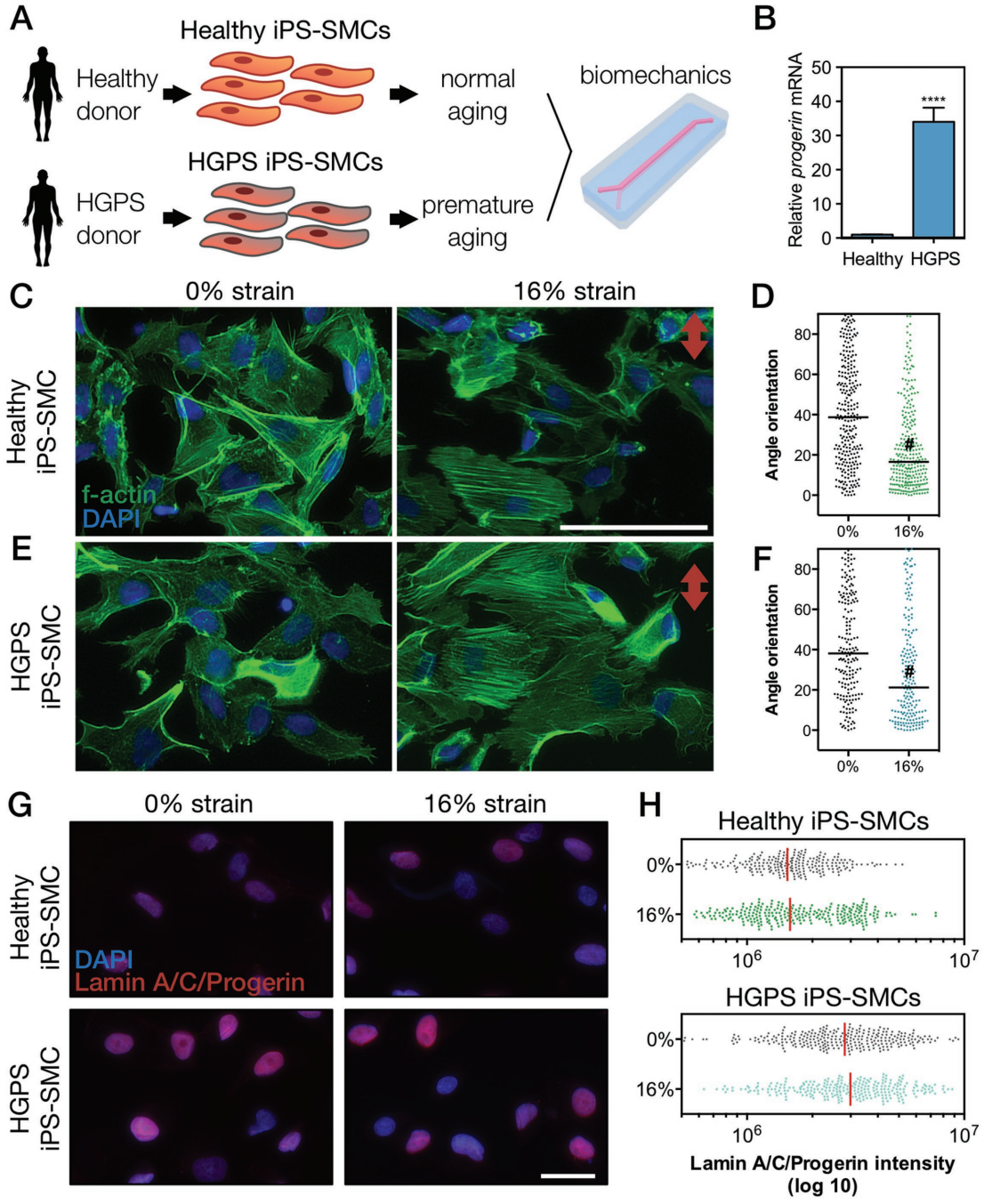

Figure 5. Biomechanical strain induces cytoskeletal reorientation of iPS-SMCs from healthy and HGPS donors. A) Schematic of the methodology used to explore biomechanical changes in a context of vascular aging. B) mRNA expression levels of progerin confirmed its overexpression HGPS cells (bars represent mean ± SD of $n = 5$). F-actin was stained for C,D) healthy or E,F) HGPS iPS-SMCs under 0% and 16% strain for 24 h and the corresponding angle orientation distribution was determined (#, $P < 0.0001$; scale bars represent 50 µm; red arrow indicates direction of strain). G) HGPS iPS-SMCs showed increase levels of lamin A/C/progerin (antibody against epitope corresponding to amino acids 231–340). H) Quantification of lamin A/C/progerin levels.

amino acids 231–340) to immunostain (Figure 5G) and quantify (Figure 5H) the combined protein levels of lamin A/C and progerin. Similar to mRNA levels, we verified also lamin A/C/progerin accumulation in HGPS iPS-SMCs as compared to healthy iPS-SMCs (Figure 5G,H). The specific accumulation of lamin A/C/progerin in the nucleus can lead to changes in the mechanical properties,[67,69] having implications for the cell response to strain.

2.5. Lovastatin and Lonafarnib Mitigated the Inflammatory Response of HGPS iPS-SMCs

Several cellular pathways are shared between aging and hypertension, resulting in vascular alterations such as remodeling, stiffness, inflammation, and oxidative stress.[70] In particular, HGPS fibroblasts are mechanically sensitive, and under conditions of mechanical stimulation show decreased

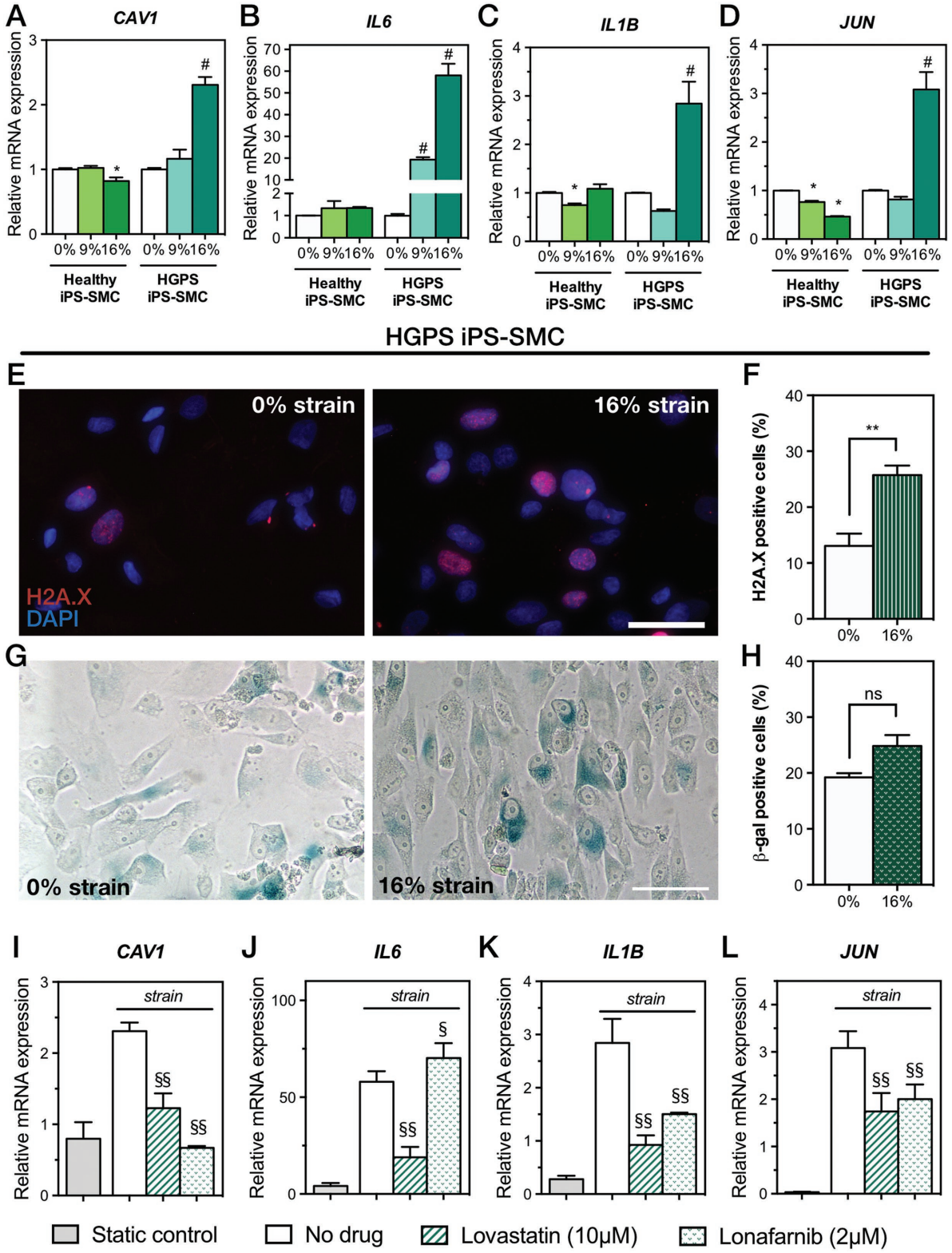

Figure 6. Exacerbated response to biomechanical strain in HGPS iPS-SMCs is rescued by lovastatin and lonafarnib. Relative mRNA expression levels of healthy and HGPS iPS-SMCs cultured under 0%, 9%, and 16% biomechanical strains for 24 h. Injury marker A) *CAV1* and inflammation markers B) *IL6*, C) *IL1B*, and D) *JUN* (*$P < 0.01$ against 0% healthy iPS-SMCs, and # indicates $P < 0.01$ against 0% HGPS iPS-SMCs; bars represent mean ± SD of $n = 5$). DNA damage was evaluated in HGPS iPS-SMCs with E) H2A.X immunostaining and F) quantified (mean ± SD of $n = 3$; **,$P = 0.0039$). Senescence was measured in HGPS iPS-SMCs via G) β-galactosidase activity staining and H) quantified (mean ± SD of $n = 3$; ns, not significant [$P = 0.0532$]). I–L) Treatment of HGPS iPS-SMCs under 16% mechanical strain with lovastatin or lonafarnib prevented increased injury and inflammatory markers, while static control on a Petri dish failed to trigger a response [(§§, $P < 0.001$; §, $P = 0.04$; compared to no drug treatment; bars for lonafarnib and lovastatin represent mean ± SD of $n = 4$; bars for static control represent mean ± SD of $n = 3$].

viability and increased apoptosis.[66] We used iPS-SMCs derived from healthy and HGPS donors, and compared the biomechanical response to strain. The markers *CAV1, IL6, IL1B*, and *JUN* (Jun Proto-Oncogene) drastically increased in HGPS iPS-SMCs under 16% strain (**Figure 6**A–D). This observation demonstrated that pathological strain elicited an exacerbated inflammatory response in HGPS iPS-SMCs that did not occur in healthy iPS-SMCs. However, we showed increased *IL6* mRNA expression in primary SMCs, but have not in healthy iPS-SMCs. *CAV1* has been identified as a marker of hypertension across different animal models[49,71] and is elevated in human serum of patients with vascular hypertension.[51,53] The increased expression of the transcriptional factor *JUN* suggested further activation of cytokines, beyond the increases in *IL6* and *IL1B*, and has been highlighted as a potential target for anti-inflammatory therapies.[72]

Together, evidence suggested that progerin accumulation in HGPS might result in increased mechanosensitivity to pathological strain and led to an exacerbated inflammatory response. The combined action of transcription factor upregulation (*JUN*) and increased proinflammatory cytokines (*IL6* and *IL1B*) suggested a cycle of propagation of inflammation that might occur in the vascular wall in HGPS patients and, at a slower pace, in physiological vascular aging. Furthermore, the observation of increased *IL6* expression, together with similar observations in two mouse models of progeria, suggested the potential role of the cytokine as a biomarker of disease. We then investigated whether exposure to pathological strain would induce further cellular damage in HGPS iPS-SMCs. DNA damage and cellular senescence have been established as hallmarks of aging,[9,73] and are upregulated in HGPS.[33,63,74,75] In our experiments, HGPS iPS-SMCs showed increased DNA damage after 24 h of biomechanical stimulation (Figure 6E,F; $P = 0.0039$). We additionally stimulated cells for 5 d under strain and observed a small increase in senescence (Figure 6G,H; $P = 0.0532$). This suggested that HGPS under dynamic pathological strain conditions altered their mRNA expression levels in favor of inflammation and vascular injury. In addition, cells presented endpoint markers of aging such as DNA damage and senescence. Importantly, chronic inflammation, which is observed in HGPS,[29] can lead to increased senescence and DNA damage[76,77] and ultimately accelerate aging.[78]

Drug treatments for HGPS primarily aim to reduce levels of progerin. These include inhibitors of the lamin-processing pathway such as 3-hydroxy-3-methylglutaryl coenzyme A (HMG-CoA; statins),[50,79,80] farnesyl transferase (FTI),[80–83] and mechanistic target of rapamycin.[84] In particular, lovastatin has been shown to improve the nuclear shape abnormalities in progeroid fibroblasts and to disrupt caveolae and decrease caveolin in SMCs.[50,79] Additionally, statins have been shown to have anti-inflammatory effects.[85–87] We then hypothesized that lovastatin treatment would mitigate changes in mRNA expression levels that were associated with strain in HGPS iPS-SMCs. Indeed, we revealed that administration of 10×10^{-6}m of lovastatin was able to rescue HGPS iPS-SMCs exacerbated injury response on the transcriptional level by preventing increases in *CAV1, IL6, IL1B,* and *JUN* (Figure 6I–L). Interestingly, 10×10^{-6} M treatment of lovastatin during 24 h under 16% strain did not reduce the levels of progerin (Figure S7, Supporting Information). Lonafarnib is a classic FTI shown to reduce levels of progerin, restore nuclear abnormalities, and improve vascular stiffness.[81,82,88] Treatment of HGPS iPS-SMCs for 24 h under 16% strain with 2×10^{-6} M of lonafarnib resulted in a decrease of progerin (Figure S7, Supporting Information), while it reduced the levels of *CAV1*, *IL1B*, and *JUN* (Figure 6I–L). However, lonafarnib failed to decrease the levels of *IL6*. This might be due to the low exposure time to lonafarnib (24 h) in comparison to other studies that have treated cells for 72 h.[81] Overall, both lovastatin and lonafarnib were able to ameliorate the exacerbated inflammatory response to strain in HGPS iPS-SMCs, with lonafarnib being more efficient in downregulating the progerin mRNA levels. Importantly, culturing HGPS iPS-SMCs under conventional cell culture systems (Petri dish) failed to trigger inflammatory and vascular injury markers (Figure 6I–L).

3. Discussion

Here, we have developed a microfluidic device that is easy to manufacture and enables the characterization of cellular responses across a range of physiological and pathological strain levels. Besides a standalone progeria-on-a-chip model, the developed device could potentially be integrated in a multi organ-on-a-chip system to provide a biomimetic vascular platform and detect system-wide effects on the vasculature. We have improved important aspects of the device design in comparison to other previously reported designs.[20,22,39,40] The fabrication methodology is simple, less expensive, and does not require highly trained operators. Our device can be conveniently scaled up to a large amount of parallel channels to serve as a high-throughput platform for vascular drug development. Additionally, the strain levels are fully characterized in situ and in silico, allowing the application of strain in a wide range. Within the device, the entire cell population can be analyzed and visualized under any conventional fluorescence microscope, and the cells can be removed from the device via trypsinization for further assays.

Using our device, we showed that primary SMCs acquire a more contractile phenotype in vitro following exposure to strain, thus better recapitulating the in vivo phenotype. Morphological changes and higher expression of *TAGLN*, *ITGB1*, and *ITGA5* suggested a more contractile phenotype and pointed toward higher mechanotransduction sensitivity via increased integrin expression.[5,42] These results are in agreement with previous reports[42,44,45] showing the alignment of SMCs under strain conditions. We next hypothesized whether a pathological strain level would induce cellular changes similar to hypertension. According to several studies, the hypertensive phenotype is characterized by an increase of mitochondrial ROS,[55–58] CAV1,[47,48] IL-6 and IL1-β[52,53] expression. The exploration of strain-magnitude unveiled a gene expression profile similar to treatment with angiotensin II, a compound known to be implicated in the development of hypertension. We indirectly assessed the

levels of ROS through mRNA expression of cytosolic and mitochondrial superoxide dismutase (*SOD1* and *SOD2*, respectively). We observed a distinct regulation of SOD1 and SOD2 depending on the strain amount. Whereas normal strain levels elicited increased expression of cytosolic superoxide dismutase, pathological strain levels elicited increased expression of mitochondrial one. By inhibiting cytosolic ROS increase with a NADPH oxidase inhibitor, we were able to specifically decrease *SOD1* under normal strain without affecting the levels of *SOD2*. This observation suggested that different strains might have distinct effects on ROS production, but further studies are required to elucidate the influence in vascular disease. Pathological levels of strain induced higher expression of vascular injury marker *CAV1*, which has been reported in patients with pulmonary hypertension,[50,51] identified in microarray screenings, and proposed as a potential target marker of hypertension.[49] Also, we observed an increase in the proinflammatory cytokine mRNA levels of *IL6* and *IL1B* under pathological strain levels. These have been implicated additionally in hypertension and aging.[52–54] Evidence suggests that pathological strain levels can indeed recapitulate some of the hallmarks observed in vascular disease and elicited by angiotensin II treatment. These alterations point to the existence of a threshold pathological strain that elicits an injury response. However, further research is required to understand the specific underlying pathways and potential identification of novel therapeutic targets, such as the Ras/MAPK/NF-κB pathways.[89]

There is a strong association between aging and cardiovascular diseases, and aging alone is the single most important risk factor for the development of cardiovascular diseases.[29,61] Additionally, inflammation is a potential mediator in the pathogenesis of several vascular diseases, including hypertension and atherosclerosis.[8,10,90] Mouse models that phenotypically recapitulate HGPS show increased activation of NF-κB with a concomitant increase in IL-6 at the transcriptional and protein levels.[91] Conversely, a mouse model of low-level chronic inflammation showed accelerated aging with increased expression of IL-6, IL1-β, and a decrease in SOD2.[78] Together, these findings highlight a potential role for inflammation and oxidative stress in the vascular wall during aging and vascular disease.[55,56] Our progeria-on-a-chip system is a crucial step toward the understanding of biomechanics of aging. HGPS targets primarily vascular cells, which are under constant mechanical stimulation. Due to lack of data specific for progeria blood vessel strain levels, we hypothesized an increase in pathological strain associated with premature aging. Here we explored a platform that combines both biomechanical stimulation and iPS-SMCs derived from HGPS patients. The HGPS iPS-SMCs expressed progerin in 15% of the cells, and were not further enriched. However, the pooled qPCR results indicated an ≈30-fold increase in progerin mRNA levels in iPS-SMCs from HGPS donors. Additionally, artificially overexpressing progerin could result in a level higher than disease, resulting in higher cell death or an over response to strain, which could reduce the relevance of the work. We showed that iPS-SMCs from both healthy and HGPS go under cytoskeletal reorientation under mechanical strain. Furthermore, we showed that HGPS-derived vascular cells demonstrated an exacerbated effect following biomechanical strain, which was unobserved using conventional planar cell culture methods (Petri dish). With this platform, we showed a unique exacerbated increase in inflammatory mRNA levels of markers *IL6*, *IL1B*, and *JUN*, as well as the vascular injury marker *CAV1*. Importantly, there is a strong link between inflammation and vascular diseases and aging, which is highlighted in the current work. We showed additionally that a statin (lovastatin) was able to prevent biomechanically induced inflammatory response, likely through anti-inflammatory effects and not directly by reducing progerin levels. Lonafarnib treatment was able to reduce levels of progerin and rescue the inflammatory and injury gene expression profiles of *IL1B*, *JUN*, and *CAV1*. However, the results suggested differences between healthy iPS-SMCs and primary SMCs, and a direct comparison might be hindered by several factors. One possible explanation for such is the different cell culture media used. The cell culture medium that maintained the iPS-SMC phenotype was smooth muscle growth medium (SmGM), being also used to expand primary SMCs. However, primary SMCs tend to dedifferentiate in culture with SmGM medium, thus requiring a starvation medium.[92] The starvation medium used for primary SMCs is less rich, while iPS-SMCs experiments were performed in a richer media (SmGM). In addition, the primary SMCs used here were from aortic origin, and might have phenotypic differences compared to a generic SMC phenotype beyond the traditional SMC markers SM-MHC and calponin. Together, these factors could explain some of the differences observed, and more research is needed to shed light onto tissue-specific SMCs differences in mechanosensitivity.

The progeria-on-a-chip system allowed the unveiling of new strain-derived in vitro mechanism that leads to increased *IL6* mRNA levels. Although the increase in *IL6* mRNA has been reported for progeria models in vivo, we showed here similar responses in vitro. We highlight the potential role of the proinflammatory cytokine IL-6 as a marker of vascular disease and potentially useful in assessing progression of HGPS. Further studies are required for the validation of IL-6 as a potential marker of disease. We hypothesize that further utilization of this platform can lead to an improved understanding of biomechanics in vascular biology. In particular, the exploration of combined effects of strain frequency, periodicity, and shear stress is expected to yield novel biological insights. Gaining deeper understanding of the molecular pathways regulating inflammation during vascular aging might pave the way for new strategies to minimizing cardiovascular risk with age. Finally, we expect the newly developed tool to serve as a standardized platform technology to study the effects of biomechanics in vascular biology, disease, and aging, while facilitating the discovery of new drugs.

4. Experimental Section

Device Fabrication: The microfluidic device was made with PDMS (Sylgard, Dow Corning) at a ratio of 10:1 (w/w) monomer to curing agent. Hard molds of the device were custom-made by laser cutting (VersaLaser) 800 µm polyoxymethylene (DuPont) sheets

and glued to the bottom of petri dishes. PDMS was cast onto the molds and cured for 24 h at 80 °C. PDMS membranes were produced by spin-coating PDMS 20:1 (w/w) on silanized silicon wafers at 950 rpm for 20 s, and cured at 80 °C for 24 h. The bottom layer PDMS slab was bonded to the PDMS membrane with oxygen plasma (Plasma Etch PE-25), and the resulting set was peeled from the wafer. The top PDMS slab was then bonded to the set of bottom-membrane with oxygen plasma and aligned manually under a microscope. The surface of the fluidic channel was treated with fibronectin (Sigma-Aldrich) at a concentration of 50 μg mL^{-1} to allow for cell attachment.

Computational Simulation: Computational finite-element models were developed using COMSOL to simulate the experimental results and to represent the mechanical deformation and allow for stress analysis of the PDMS membrane. The device structure was modeled as two PDMS flexible bodies sandwiching a flexible PDMS membrane with a thickness of 100 μm. The Young's moduli used were 2.5 MPa for the flexible bodies and 500 kPa for the membrane, respectively, as determined from mechanical characterization by Instron tensile mechanical measurements. The Poisson's ratio used for both PDMS compositions was 0.49.[93] The interfaces between the different PDMS layers were modeled as a bonded contact. The base of the model was constrained as fixed and a linearly increasing pressure, ranging from 0 to 50 kPa, was applied to the top surface of the PDMS membrane. The simulation took into account the presence of SMCs, which were uniformly distributed along the top surface of the membrane. The interfaces between the cells and the membrane were modeled as a bonded contact. The cells were shaped according to a morphological evaluation of in vitro studies through confocal imaging.[94] For the cells, literature values for the Elastic modulus (100 kPa) and the Poisson's ratio (0.49) were used.[95] The strains generated on the top surface of the membrane, as well as on the cells attached to the membrane surface, were analyzed.

Mechanical Stimulation: Cells were stimulated for 24 h with different percentages of cyclic strain. To ensure media exchange, the fluidic channel was perfused with cell culture media at a flow rate of 100 μL h^{-1}. To stimulate the cells, the vacuum inlet of the microfluidic pump was connected to a computer-controlled solenoid system and stimulated at a frequency of 0.5 Hz. The vacuum pressure was adjusted with a pressure regulator and used in the range of 0 kPa (= 0% strain), 10 kPa (= 9% strain), and 20 kPa (= 16% strain).

Cell Culture: Aortic SMCs (Lonza) were grown in Smooth Muscle Growth Media-2 BulletKit (Lonza) at 37 °C and 5% CO_2 in a humidified incubator. Cells were trypsinized from cell culture flasks and seeded in the microfluidic channels at a density of 1.6 million cells mL^{-1}. Prior to the start of strain experiments, cells were maintained in media containing DMEM/F12 1:1 mixture (Thermo Fisher Scientific) supplemented with insulin–transferrin–selenium (Thermo Fisher Scientific).[92] iPS generated from healthy and HGPS donors were kindly provided by Xavier Nissan and previously characterized.[35] Differentiation was performed according to a previously described protocol.[64] At the end, 95% of both differentiated cells expressed a-SMA, SMMHC, and calponin proteins. Moreover, HGPS-iPSC SMCs expressed progerin protein (15% of the cells). Healthy and HGPS iPS-derived SMCs were grown in SmGM-2 media at 37 °C and 5% CO_2 in a humidified incubator. Due to the smaller size, iPS-SMCs were seeded in the microfluidic device at a density of 3.2 million cells mL^{-1}, which yielded a cell confluence that was identical to those used for the SMCs. Treatment with 10×10^{-6} M lovastatin (Sigma-Aldrich) was administered 2 h before the start of mechanical stimulation and continued through the 24 h of cyclic strain. Treatment with 2×10^{-6} M lonafarnib (Sigma-Aldrich) was administered together with mechanical stimulation and continued through the 24 h of cyclic strain.

Gene Expression: Cells were trypsinized from the microfluidic devices 24 h after mechanical stimulation. RNA was extracted using an RNeasy Micro kit (Qiagen). cDNA was synthesized from a total of 500 ng of RNA using the QuantiTec Reverse Transcription kit (Qiagen) following the manufacturer's protocol. qRT-PCR was performed in an iQ5 thermocycler using SYBR green probe (Biorad). Gene expressions were normalized using housekeeping glyceraldehide 3-phosphate dehydrogenase (GAPDH). All used primer sequences are listed in Table S1 (Supporting Information). Results follow the $2^{-\Delta\Delta Ct}$ method and are reported as fold change as compared with the no strain (0%) control, unless otherwise indicated.

Immunocytochemistry: Cells were immediately fixed in 4% paraformaldehyde (Sigma-Aldrich) for 15 min at room temperature. Cells were then permeabilized with 1% (v/v) Triton X-100 (Sigma-Aldrich) for 10 min, followed by blocking with 1% bovine albumin serum (Sigma-Aldrich) for 45 min at room temperature. Primary antibody against lamin A/C (Santa Cruz, sc-20681; 1:50; reacts against both lamin A/C and progerin) was incubated at room temperature for 1 h. Primary antibody against the phosphor–histone H2A.X (Cell Signaling Technology, 9718, 1:400) was incubated overnight at 4 °C. The channels were washed with phosphate buffer saline (PBS; Thermo Fisher Scientific) five times and solutions of fluorescently labeled secondary antibodies were introduced (Alexa 546 anti-mouse, Thermo Fisher Scientific; Alexa 594 anti-rabbit, Thermo Fisher Scientific). Secondary antibodies were incubated for 1 h and nuclei counterstained with 4′,6-diamidino-2-phenyllindole (DAPI) (Thermo Fisher Scientific) for 5 min. F-actin staining was achieved by incubating cells with Alexa 488 phalloidin solution according to manufacturer's protocol. Images were acquired with a Zeiss Observer D1 microscope.

Cell Senescence: Senescent cells (n = 3 experiments) were detected through histochemical staining of β-galactosidase (Senescence Cells Histochemical Staining Kit, Sigma-Aldrich) according to the manufacturer's protocol. Briefly, after 5 d of cyclic mechanical stimulation, cells were washed with PBS and fixed with 1X fixation buffer for 7 min at room temperature. The staining 5-bromo-4-chloro-3-indolyl-β-D-galactopyranoside (X-Gal) solution was prepared accordingly and the cells were incubated for 24 h at 37 °C. Stained cells were washed in PBS and imaged on an inverted bright field microscope.

Image Quantification: Cell orientation, length, and width were determined from n = 3 experiments of F-actin stained cells. Three microscopic images for each n were analyzed in ImageJ to determine angle of orientation, length, and width. Nuclei images obtained after computer simulations were used to determine the vector displacement maps upon strain, using the Particle Image Velocimetry plugin of ImageJ.

Statistical Analysis: Results are presented as mean ± standard deviation (SD) unless otherwise indicated. Group data analysis was performed with one-way ANOVA and a Tukey's post hoc test

against control group. Comparison between two groups was performed using a student's *t*-test.

Supporting Information

Supporting Information is available from the Wiley Online Library or from the author.

Acknowledgements

The authors gratefully acknowledge funding by the Defense Threat Reduction Agency (DTRA) under Space and Naval Warfare Systems Center Pacific (SSC PACIFIC) Contract No. N66001-13-C-2027. The authors also acknowledge funding from the Office of Naval Research Young National Investigator Award, the National Institutes of Health (EB012597, AR057837, DE021468, HL099073, and R56AI105024), and the Presidential Early Career Award for Scientists and Engineers (PECASE). The publication of this material does not constitute approval by the government of the findings or conclusions herein. J.R. acknowledges the support from the Portuguese Foundation for Science and Technology (SFRH/BD/51679/2011). J.L. acknowledges financial support from Innovative Research Incentives Scheme Veni No. 14328 of the Netherlands Organization for Scientific Research (NWO). J.R. acknowledges financial support by the People Programme (Marie Curie Actions) under REA Grant Agreement No. 622294 (PreVascIn). X.N. acknowledges financial support by the Assocation Française contre les Myopathies (AFM-Telethon), INSERM, the region Ile-de-France (DIM-biotherapies), the National Infrastructure (INGESTEM) and Genopole. The authors declare no conflict of interest.

[1] M. J. Davis, M. A. Hill, *Physiol. Rev.* **1999**, *79*, 387.
[2] C. Stefanadis, C. Stratos, C. Vlachopoulos, S. Marakas, H. Boudoulas, I. Kallikazaros, E. Tsiamis, K. Toutouzas, L. Sioros, P. Toutouzas, *Circulation* **1995**, *92*, 2210.
[3] B. Williams, *J. Hypertens.* **1998**, *16*, 1921.
[4] M. A. Anwar, J. Shalhoub, C. S. Lim, M. S. Gohel, A. H. Davies, *J. Vasc. Res.* **2012**, *49*, 463.
[5] E. H. Heerkens, A. S. Izzard, A. M. Heagerty, *Hypertension* **2007**, *49*, 1.
[6] S. S. Rensen, P. A. Doevendans, G. J. van Eys, *Netherlands Heart J.* **2007**, *15*, 100.
[7] D. Lu, G. S. Kassab, *J. R. Soc., Interface* **2011**, *8*, 1379.
[8] C. Savoia, E. L. Schiffrin, *Curr. Opin. Nephrol. Hypertens.* **2006**, *15*, 152.
[9] C. Lopez-Otin, M. A. Blasco, L. Partridge, M. Serrano, G. Kroemer, *Cell* **2013**, *153*, 1194.
[10] M. Maggio, J. M. Guralnik, D. L. Longo, L. Ferrucci, *J. Gerontol., Ser. A* **2006**, *61*, 575.
[11] W. J. Polacheck, R. Li, S. G. Uzel, R. D. Kamm, *Lab Chip* **2013**, *13*, 2252.
[12] S. N. Bhatia, D. E. Ingber, *Nat. Biotechnol.* **2014**, *32*, 760.
[13] J. Ribas, H. Sadeghi, A. Manbachi, J. Leijten, K. Brinegar, Y. S. Zhang, L. Ferreira, A. Khademhosseini, *Appl. In Vitro Toxicol.* **2016**, *2*, 82.
[14] D. Huh, B. D. Matthews, A. Mammoto, M. Montoya-Zavala, H. Y. Hsin, D. E. Ingber, *Science* **2010**, *328*, 1662.
[15] D. Huh, D. C. Leslie, B. D. Matthews, J. P. Fraser, S. Jurek, G. A. Hamilton, K. S. Thorneloe, M. A. McAlexander, D. E. Ingber, *Sci. Transl. Med.* **2012**, *4*, 159ra147.
[16] N. J. Douville, P. Zamankhan, Y. C. Tung, R. Li, B. L. Vaughan, C. F. Tai, J. White, P. J. Christensen, J. B. Grotberg, S. Takayama, *Lab Chip* **2011**, *11*, 609.
[17] H. J. Kim, D. Huh, G. Hamilton, D. E. Ingber, *Lab Chip* **2012**, *12*, 2165.
[18] H. J. Kim, D. E. Ingber, *Integr. Biol.* **2013**, *5*, 1130.
[19] H. J. Kim, H. Li, J. J. Collins, D. E. Ingber, *Proc. Natl. Acad. Sci. USA* **2016**, *113*, E7.
[20] J. Lee, M. Wong, Q. Smith, A. B. Baker, *Lab Chip* **2013**, *13*, 4573.
[21] Y. Shao, X. Tan, R. Novitski, M. Muqaddam, P. List, L. Williamson, J. Fu, A. P. Liu, *Rev. Sci. Instrum.* **2013**, *84*, 114304.
[22] R. Sinha, S. Le Gac, N. Verdonschot, A. van den Berg, B. Koopman, J. Rouwkema, *Lab Chip* **2015**, *15*, 429.
[23] D. Meza, L. Abejar, D. A. Rubenstein, W. Yin, *J. Biomech. Eng.* **2016**, *138*, 031007.
[24] W. Zhang, Y. S. Zhang, S. M. Bakht, J. Aleman, S. R. Shin, K. Yue, M. Sica, J. Ribas, M. Duchamp, J. Ju, R. B. Sadeghian, D. Kim, M. R. Dokmeci, A. Atala, A. Khademhosseini, *Lab Chip* **2016**, *16*, 1579.
[25] J. Zhang, Q. Lian, G. Zhu, F. Zhou, L. Sui, C. Tan, R. A. Mutalif, R. Navasankari, Y. Zhang, H. F. Tse, C. L. Stewart, A. Colman, *Cell Stem Cell* **2011**, *8*, 31.
[26] A. De Sandre-Giovannoli, R. Bernard, P. Cau, C. Navarro, J. Amiel, I. Boccaccio, S. Lyonnet, C. L. Stewart, A. Munnich, M. Le Merrer, N. Levy, *Science* **2003**, *300*, 2055.
[27] M. Eriksson, W. T. Brown, L. B. Gordon, M. W. Glynn, J. Singer, L. Scott, M. R. Erdos, C. M. Robbins, T. Y. Moses, P. Berglund, A. Dutra, E. Pak, S. Durkin, A. B. Csoka, M. Boehnke, T. W. Glover, F. S. Collins, *Nature* **2003**, *423*, 293.
[28] M. V. Blagosklonny, *Aging* **2011**, *3*, 685.
[29] M. Olive, I. Harten, R. Mitchell, J. K. Beers, K. Djabali, K. Cao, M. R. Erdos, C. Blair, B. Funke, L. Smoot, M. Gerhard-Herman, J. T. Machan, R. Kutys, R. Virmani, F. S. Collins, T. N. Wight, E. G. Nabel, L. B. Gordon, *Arterioscler., Thromb., Vasc. Biol.* **2010**, *30*, 2301.
[30] C. R. Burtner, B. K. Kennedy, *Nat. Rev. Mol. Cell Biol.* **2010**, *11*, 567.
[31] M. A. Merideth, L. B. Gordon, S. Clauss, V. Sachdev, A. C. Smith, M. B. Perry, C. C. Brewer, C. Zalewski, H. J. Kim, B. Solomon, B. P. Brooks, L. H. Gerber, M. L. Turner, D. L. Domingo, T. C. Hart, J. Graf, J. C. Reynolds, A. Gropman, J. A. Yanovski, M. Gerhard-Herman, F. S. Collins, E. G. Nabel, R. O. Cannon 3rd, W. A. Gahl, W. J. Introne, *N. Engl. J. Med.* **2008**, *358*, 592.
[32] D. McClintock, L. B. Gordon, K. Djabali, *Proc. Natl. Acad. Sci. USA* **2006**, *103*, 2154.
[33] G. H. Liu, B. Z. Barkho, S. Ruiz, D. Diep, J. Qu, S. L. Yang, A. D. Panopoulos, K. Suzuki, L. Kurian, C. Walsh, J. Thompson, S. Boue, H. L. Fung, I. Sancho-Martinez, K. Zhang, J. Yates 3rd, J. C. Izpisua Belmonte, *Nature* **2011**, *472*, 221.
[34] O. Dreesen, C. L. Stewart, *Aging* **2011**, *3*, 889.
[35] X. Nissan, S. Blondel, C. Navarro, Y. Maury, C. Denis, M. Girard, C. Martinat, A. De Sandre-Giovannoli, N. Levy, M. Peschanski, *Cell Rep.* **2012**, *2*, 1.
[36] J. A. Brassard, N. Fekete, A. Garnier, C. A. Hoesli, *Biogerontology* **2016**, *17*, 129.
[37] S. Blondel, A. L. Egesipe, P. Picardi, A. L. Jaskowiak, M. Notarnicola, J. Ragot, J. Tournois, A. Le Corf, B. Brinon, P. Poydenot, P. Georges, C. Navarro, P. R. Pitrez, L. Ferreira, G. Bollot, C. Bauvais, D. Laustriat, A. Mejat, A. De Sandre-Giovannoli, N. Levy, M. Bifulco, M. Peschanski, X. Nissan, *Cell Death Dis.* **2016**, *7*, e2105.

[38] G. S. Ugolini, M. Rasponi, A. Pavesi, R. Santoro, R. Kamm, G. B. Fiore, M. Pesce, M. Soncini, *Biotechnol. Bioeng.* **2016**, *113*, 859.
[39] W. Zheng, R. Huang, B. Jiang, Y. Zhao, W. Zhang, X. Jiang, *Small* **2016**, *12*, 2022.
[40] M. Aragona, T. Panciera, A. Manfrin, S. Giulitti, F. Michielin, N. Elvassore, S. Dupont, S. Piccolo, *Cell* **2013**, *154*, 1047.
[41] J. Zhou, L. E. Niklason, *Integr. Biol.* **2012**, *4*, 1487.
[42] E. Wilson, K. Sudhir, H. E. Ives, *J. Clin. Invest.* **1995**, *96*, 2364.
[43] A. M. Greiner, H. Chen, J. P. Spatz, R. Kemkemer, *PloS One* **2013**, *8*, e77328.
[44] B. Liu, M. J. Qu, K. R. Qin, H. Li, Z. K. Li, B. R. Shen, Z. L. Jiang, *Biophys. J.* **2008**, *94*, 1497.
[45] S. Albinsson, I. Nordstrom, P. Hellstrand, *J. Biol. Chem.* **2004**, *279*, 34849.
[46] M. Bader, J. Peters, O. Baltatu, D. N. Muller, F. C. Luft, D. Ganten, *J. Mol. Med.* **2001**, *79*, 76.
[47] C. D. Hardin, J. Vallejo, *Cardiovasc. Res.* **2006**, *69*, 808.
[48] J. Yu, S. Bergaya, T. Murata, I. F. Alp, M. P. Bauer, M. I. Lin, M. Drab, T. V. Kurzchalia, R. V. Stan, W. C. Sessa, *J. Clin. Invest.* **2006**, *116*, 1284.
[49] T. H. Grayson, S. J. Ohms, T. D. Brackenbury, K. R. Meaney, K. Peng, Y. E. Pittelkow, S. R. Wilson, S. L. Sandow, C. E. Hill, *BMC Genomics* **2007**, *8*, 404.
[50] H. H. Patel, S. Zhang, F. Murray, R. Y. Suda, B. P. Head, U. Yokoyama, J. S. Swaney, I. R. Niesman, R. T. Schermuly, S. S. Pullamsetti, P. A. Thistlethwaite, A. Miyanohara, M. G. Farquhar, J. X. Yuan, P. A. Insel, *FASEB J.* **2007**, *21*, 2970.
[51] K. Y. Wang, M. F. Lee, H. C. Ho, K. W. Liang, C. C. Liu, W. J. Tsai, W. W. Lin, *BioMed Res. Int.* **2015**, *2015*, 173970.
[52] L. E. Bautista, L. M. Vera, I. A. Arenas, G. Gamarra, *J. Hum. Hypertens.* **2005**, *19*, 149.
[53] M. Humbert, G. Monti, F. Brenot, O. Sitbon, A. Portier, L. Grangeot-Keros, P. Duroux, P. Galanaud, G. Simonneau, D. Emilie, *Am. J. Respir. Crit. Care Med.* **1995**, *151*, 1628.
[54] S. M. Golembeski, J. West, Y. Tada, K. A. Fagan, *Chest* **2005**, *128*, 572S.
[55] S. R. Datla, K. K. Griendling, *Hypertension* **2010**, *56*, 325.
[56] T. M. Paravicini, R. M. Touyz, *Diabetes Care* **2008**, *31*, S170.
[57] M. Kojima, I. Shiojima, T. Yamazaki, I. Komuro, Z. Zou, Y. Wang, T. Mizuno, K. Ueki, K. Tobe, T. Kadowaki, *Circulation* **1994**, *89*, 2204.
[58] R. Kranzhofer, J. Schmidt, C. A. Pfeiffer, S. Hagl, P. Libby, W. Kubler, *Arterioscler., Thromb., Vasc. Biol.* **1999**, *19*, 1623.
[59] H. ten Freyhaus, M. Huntgeburth, K. Wingler, J. Schnitker, A. T. Baumer, M. Vantler, M. M. Bekhite, M. Wartenberg, H. Sauer, S. Rosenkranz, *Cardiovasc. Res.* **2006**, *71*, 331.
[60] K. Kappert, G. Schmidt, G. Doerr, B. Wollert-Wulf, E. Fleck, K. Graf, *Hypertension* **2000**, *35*, 255.
[61] B. J. North, D. A. Sinclair, *Circ. Res.* **2012**, *110*, 1097.
[62] J. L. Sterneckert, P. Reinhardt, H. R. Scholer, *Nat. Rev. Genet.* **2014**, *15*, 625.
[63] P. Cau, C. Navarro, K. Harhouri, P. Roll, S. Sigaudy, E. Kaspi, S. Perrin, A. De Sandre-Giovannoli, N. Levy, *Semin. Cell Dev. Biol.* **2014**, *29*, 125.
[64] H. Vazao, R. P. das Neves, M. Graos, L. Ferreira, *PloS One* **2011**, *6*, e17771.
[65] K. N. Dahl, A. J. Ribeiro, J. Lammerding, *Circ. Res.* **2008**, *102*, 1307.
[66] V. L. Verstraeten, J. Y. Ji, K. S. Cummings, R. T. Lee, J. Lammerding, *Aging Cell* **2008**, *7*, 383.
[67] R. D. Goldman, D. K. Shumaker, M. R. Erdos, M. Eriksson, A. E. Goldman, L. B. Gordon, Y. Gruenbaum, S. Khuon, M. Mendez, R. Varga, F. S. Collins, *Proc. Natl. Acad. Sci. USA* **2004**, *101*, 8963.
[68] K. Cao, C. D. Blair, D. A. Faddah, J. E. Kieckhaefer, M. Olive, M. R. Erdos, E. G. Nabel, F. S. Collins, *J. Clin. Invest.* **2011**, *121*, 2833.
[69] K. N. Dahl, P. Scaffidi, M. F. Islam, A. G. Yodh, K. L. Wilson, T. Misteli, *Proc. Natl. Acad. Sci. USA* **2006**, *103*, 10271.
[70] A. Harvey, A. C. Montezano, R. M. Touyz, *J. Mol. Cell. Cardiol.* **2015**, *83*, 112.
[71] E. D. Austin, L. Ma, C. LeDuc, E. Berman Rosenzweig, A. Borczuk, J. A. Phillips 3rd, T. Palomero, P. Sumazin, H. R. Kim, M. H. Talati, J. West, J. E. Loyd, W. K. Chung, *Circ. Cardiovasc. Genet.* **2012**, *5*, 336.
[72] R. G. Fahmy, A. Waldman, G. Zhang, A. Mitchell, N. Tedla, H. Cai, C. R. Geczy, C. N. Chesterman, M. Perry, L. M. Khachigian, *Nat. Biotechnol.* **2006**, *24*, 856.
[73] M. Collado, M. A. Blasco, M. Serrano, *Cell* **2007**, *130*, 223.
[74] L. Trigueros-Motos, J. M. Gonzalez, J. Rivera, V. Andres, *Front. Biosci.* **2011**, *3*, 1285.
[75] H. Endisha, J. Merrill-Schools, M. Zhao, M. Bristol, X. Wang, N. Kubben, L. W. Elmore, *Pathobiology* **2015**, *82*, 9.
[76] J. C. Acosta, A. O'Loghlen, A. Banito, M. V. Guijarro, A. Augert, S. Raguz, M. Fumagalli, M. Da Costa, C. Brown, N. Popov, Y. Takatsu, J. Melamed, F. d'Adda di Fagagna, D. Bernard, E. Hernando, J. Gil, *Cell* **2008**, *133*, 1006.
[77] T. Kuilman, C. Michaloglou, L. C. Vredeveld, S. Douma, R. van Doorn, C. J. Desmet, L. A. Aarden, W. J. Mooi, D. S. Peeper, *Cell* **2008**, *133*, 1019.
[78] D. Jurk, C. Wilson, J. F. Passos, F. Oakley, C. Correia-Melo, L. Greaves, G. Saretzki, C. Fox, C. Lawless, R. Anderson, G. Hewitt, S. L. Pender, N. Fullard, G. Nelson, J. Mann, B. van de Sluis, D. A. Mann, T. von Zglinicki, *Nat. Commun.* **2014**, *2*, 4172.
[79] M. Bifulco, A. D'Alessandro, S. Paladino, A. M. Malfitano, M. Notarnicola, M. G. Caruso, C. Laezza, *FEBS J.* **2013**, *280*, 6223.
[80] I. Varela, S. Pereira, A. P. Ugalde, C. L. Navarro, M. F. Suarez, P. Cau, J. Cadinanos, F. G. Osorio, N. Foray, J. Cobo, F. de Carlos, N. Levy, J. M. Freije, C. Lopez-Otin, *Nat. Med.* **2008**, *14*, 767.
[81] B. C. Capell, M. R. Erdos, J. P. Madigan, J. J. Fiordalisi, R. Varga, K. N. Conneely, L. B. Gordon, C. J. Der, A. D. Cox, F. S. Collins, *Proc. Natl. Acad. Sci. USA* **2005**, *102*, 12879.
[82] S. H. Yang, M. Meta, X. Qiao, D. Frost, J. Bauch, C. Coffinier, S. Majumdar, M. O. Bergo, S. G. Young, L. G. Fong, *J. Clin. Invest.* **2006**, *116*, 2115.
[83] A. Marcuzzi, L. De Leo, G. Decorti, S. Crovella, A. Tommasini, A. Pontillo, *Pediatr. Res.* **2011**, *70*, 78.
[84] K. Cao, J. J. Graziotto, C. D. Blair, J. R. Mazzulli, M. R. Erdos, D. Krainc, F. S. Collins, *Sci. Transl. Med.* **2011**, *3*, 89ra58.
[85] M. K. Jain, P. M. Ridker, *Nat. Rev. Drug Discovery* **2005**, *4*, 977.
[86] U. Schonbeck, P. Libby, *Circulation* **2004**, *109*, II18.
[87] G. Weitz-Schmidt, *Trends Pharmacol. Sci.* **2002**, *23*, 482.
[88] L. B. Gordon, M. E. Kleinman, D. T. Miller, D. S. Neuberg, A. Giobbie-Hurder, M. Gerhard-Herman, L. B. Smoot, C. M. Gordon, R. Cleveland, B. D. Snyder, B. Fligor, W. R. Bishop, P. Statkevich, A. Regen, A. Sonis, S. Riley, C. Ploski, A. Correia, N. Quinn, N. J. Ullrich, A. Nazarian, M. G. Liang, S. Y. Huh, A. Schwartzman, M. W. Kieran, *Proc. Natl. Acad. Sci. USA* **2012**, *109*, 16666.
[89] A. Zampetaki, Z. Zhang, Y. Hu, Q. Xu, *Am. J. Physiol.: Heart Circ. Physiol.* **2005**, *288*, H2946.
[90] D. G. Harrison, T. J. Guzik, H. E. Lob, M. S. Madhur, P. J. Marvar, S. R. Thabet, A. Vinh, C. M. Weyand, *Hypertension* **2011**, *57*, 132.
[91] F. G. Osorio, C. Barcena, C. Soria-Valles, A. J. Ramsay, F. de Carlos, J. Cobo, A. Fueyo, J. M. Freije, C. Lopez-Otin, *Genes Dev.* **2012**, *26*, 2311.
[92] P. Libby, K. V. O'Brien, *J. Cell. Physiol.* **1983**, *115*, 217.
[93] R. H. Pritchard, P. Lava, D. Debruyne, E. M. Terentjev, *Soft Matter* **2013**, *9*, 6037.
[94] B. G. Miller, V. H. Gattone 2nd, J. M. Overhage, H. G. Bohlen, A. P. Evan, *Anat. Rec.* **1986**, *216*, 95.
[95] K. D. Costa, *Dis. Markers* **2003**, *19*, 139.

Received: November 7, 2016
Revised: January 2, 2017
Published online:

